

INFLUENCE OF HIGH Sr²⁺ SUBSTITUTION ON THE STRUCTURE AND PHOTOCATALYTIC ACTIVITY OF Ba_{1-x}Sr_xTiO₃ FOR DYE DEGRADATION

Dianisa Khoirum Sandi*1, Trya Andini2, Fahru Nurosyid2, and Yofentina Iriani2

¹Study Program of Energy Conversion Engineering, Department of Mechanical Engineering, Politeknik Negeri Semarang, 50275, Semarang, Indonesia

²Department of Physics, Faculty of Mathematics and Natural Sciences, Universitas Sebelas Maret, Surakarta, 57126, Indonesia

*dianisa.khoirumsandi@polines.ac.id

Received 2025-08-04, Revised 2025-10-02, Accepted 2025-10-16, Available Online 2025-10-16, Published Regularly October 2025

ABSTRACT

Barium strontium titanate or BST (Ba_{1-x}Sr_xTiO₃) photocatalysts with distinct Sr substitutions (x = 0.5, 0.6, 0.7, and 0.8) were fabricated using the co-precipitation technique. This study aimed to investigate the influence of the high Sr²⁺ contents on the structural property and photocatalytic activity to identify the optimal composition. X-ray diffraction (XRD analysis) confirmed cubic BST formation at all Sr concentrations and reduced lattice constants with increasing Sr²⁺ contents. Fourier transform infra-red (FTIR) investigation also validated the formation of the prepared BST with different Sr contents. The photocatalytic activity of the BST photocatalysts was evaluated by the degradation of methylene blue (MB) under UV light irradiation. Notably, the photocatalytic efficiency improved at x=0.5 to x=0.7, attributed to enhanced lattice distortion induced by Sr substitution. However, a further increase of x = 0.8 resulted in reduced photocatalytic activity, likely due to the formation of a more symmetric structure and reduced crystal distortion. Ba_{0.3}Sr_{0.7}TiO₃ exhibited the highest degradation rate (41%) among all samples tested. The results suggest that the high Sr level critically affects the structural properties and photocatalytic efficiency of BST and underline x = 0.7 as the optimal composition for photocatalytic applications.

Keywords: barium strontium titanate; Sr substitution; methylene blue; structural property; photocatalytic activity

INTRODUCTION

The rising energy demand and environmental emergencies have induced significant concern in photocatalysis, whether for hydrogen production via water splitting or pollutant degradation using light exposure^[1, 2]. Photocatalysis is a process in which light (UV or visible) is absorbed by a photocatalyst, resulting in charge separations (electrons and holes). The electron-hole pairs stimulate a reduction-oxidation reaction that can produce hydrogen or degraded pollutants^[3-5]. The role of photocatalyst materials is significant in photocatalysis. Generally, oxides have been at the forefront of photocatalyst materials since they are nonhazardous, low-cost, and stable^[6, 7]. Among the oxides, titanates are preferable as they can be easily engineered to obtain improved properties, primarily through doping^[8].

Particularly, Barium Titanate (BaTiO₃ or BTO) is one titanate from ferroelectric semiconductors with a band gap of about 3.2–3.5 eV^[2, 9-11]. Its beneficial features include high

oxygen vacancy, tunable size and morphology, spontaneous polarization, rapid migration of photogenerated charge carriers, and band bending^[9, 12, 13]. These features make it suitable for photocatalytic applications^[12, 13]. The chemical stability and ferroelectric nature of this material promote better charge separation, which is advantageous for the photocatalytic process^[2, 14]. Despite its great potential, challenges such as low efficiency under visible light and fast electron-hole recombination still need to be overcome through further material engineering^[15]. BTO is often modified through doping (e.g., with Sr^[15], Co^[13], La^[3], Ag^[1], Bi^[2], or Rh^[16]), composite formation with other photocatalysts such as TiO₂ and STO^[17], and morphology engineering to increase its photocatalytic activity^[9, 15]. With appropriate development, BTO could become a more effective photocatalyst for environmental and renewable energy applications.

Barium strontium titanate or BST ($Ba_{1-x}Sr_xTiO_3$, 0< x<1) is the modification form of BTO with partial substitution of Ba^{2+} ions with Sr^{2+} [5, 18]. The main differences between the two are the band gap and ferroelectric properties. BTO has a band gap of around 3.2–3.5 eV, limiting the UV light absorption [19-21]. Meanwhile, BST has the advantage of band gap alteration by replacing part of the Ba^{2+} ions with Sr^{2+} , thereby enhancing visible light absorption and improving the efficiency of electron-hole charge separation [8, 22]. In addition, BST exhibits superior dielectric and ferroelectric properties, which can help reduce electron-hole recombination and enhance photocatalytic activity [23, 24]. BST with the right Sr composition can have a smaller band gap, enhancing its visible light absorption and increasing its photocatalytic efficiency [17]. In addition, adding Sr lowers the ferroelectric transition temperature and increases the mobility of charge carriers, which is essential in photocatalytic applications [25]. Nevertheless, the main challenges in its use are operational stability and optimization of the Ba/Sr ratio to achieve the best photocatalytic properties.

The distinct Ba/Sr ratios can change the microstructure of BST, which further modifies its physical, chemical, and optical properties and photocatalytic activity. Mohan et al. [17] synthesized BaTiO3@SrTiO3 core-shell nanowires by varying Sr/Ba ratios. The yields showed that increasing Sr content increased the surface area and charge separation efficiency, enhancing hydrogen production via sono-photocatalysis. Liu et al. [26] demonstrated that Sr doping into BaTiO3 contributed to improving the tribocatalytic performance in degrading organic pollutants. The study showed that Sr substitution of up to 20% increased the degradation efficiency of Rhodamine B (RhB) by about 35%, attributed to the increase in charge transfer efficiency due to Sr doping. Liu et al. [27] fabricated Ba1-xSrxTiO3 with the solgel assisted solid phase method and observed the effects of the Ba/Sr ratio on the microstructure and photocatalytic activity. The results revealed that the carrier recombination rate gradually increased with an increasing Ba content, and the Ba/Sr ratio of 0.7/0.3 exhibited the smallest bandgap (Eg = 3.027 eV) and had the largest photocatalytic hydrogen production rate.

Research on the photocatalytic activity of BST is still limited and needs to be explored. Up to now, there has been a lack of investigation of the influences of the distinct Ba/Sr ratios on the structure and photocatalytic activity of BST, especially at high Sr levels and for organic dye degradation applications. Accordingly, this study attempted to synthesize $Ba_{1-x}Sr_xTiO_3$ (x=0.5, 0.6, 0.7, and 0.8) via the co-precipitation method. Besides, the novelty of this research was on the use of the high Sr doping of > 0.5, where other studies were commonly conducted at < 0.5 and even < 0.1. The prepared BST was employed as a photocatalyst to degrade methylene blue (MB) pollutants.

Hence, this study aimed to investigate the influence of variations in high Sr²⁺substitution on the structural property and photocatalytic activity of Ba_{1-x}Sr_xTiO₃. This study also determined

the optimal Sr substitution composition that yields the highest photocatalytic efficiency in methylene blue (MB) degradation under UV light. The findings are expected to be a valuable reference for developing and modifying BST-based photocatalysts, not only for dye degradation but also for potential applications in photocatalytic hydrogen production.

METHOD

Materials

The raw materials included barium hydroxide [Ba(OH)₂] (Sigma Aldrich, 95%), titanium tetra butoxide [Ti(C₄H₉O)₄] (Sigma Aldrich, 97%), oxalic acid (C₂H₂O₄) (Sigma Aldrich \geq 99%), strontium nitrate [Sr(NO₃)₂] (Sigma Aldrich, 95%), and Isopropanol (IPA) (Sigma Aldrich, 95%).

Ba_{1-x}Sr_xTiO₃ Preparation

BST samples were prepared using the co-precipitation method. First, all raw materials were weighed following the stoichiometry formula of $Ba_{1-x}Sr_xTiO_3$ (x=0.5, 0.6, 0.7, and 0.8). Oxalic acid was dissolved in IPA by stirring with a magnetic stirrer at 250 rpm for 20 minutes (Solution O). Separately, barium hydroxide was diluted in IPA by stirring at 250 rpm for 30 minutes (Solution B). With the same procedure, titanium tetra butoxide was dissolved in IPA (Solution T). Solution T was mixed with Solution O by stirring at 250 rpm for 20 minutes. The mixture was then added with Solution B and strontium nitrate and stirred for 30 minutes. In this step, the masses of strontium nitrate were varied following the desired mol content (x). The resulting solution was added with distilled water, stirred for 1 hour using a magnetic stirrer, and left for 24 hours. The precipitated solution was then washed three times, once using ethanol and twice with distilled water. After that, the precipitate was filtered using filter paper and hydrolyzed for 10 hours at 100° C to obtain powder form. Finally, the powder sample was sintered at 1000° C for 4 hours, producing the $Ba_{1-x}Sr_xTiO_3$ powder samples.

Characterizations

Fourier Transform Infrared (FTIR) spectroscopy (Shimadzu A21004802518) was utilized to identify the functional groups present within the samples in the wavenumber range of 350 – 4000 cm⁻¹. Besides, X-ray diffraction (XRD) analysis was conducted using a Bruker D8 Advance diffractometer with a Cu K α radiation source (λ = 1.5406 Å) to investigate their crystalline structure. The XRD data were then exploited to estimate the crystallite size of the samples through the Debye-Scherrer equation, as shown in Equation 1. In which D, k, β , θ , and λ are the crystallite size (nm), the Scherrer constant (0.94), the value of Full Width at Half Maximum (FWHM) (rad), the diffraction angle (degrees), and the wavelength of the Cu XRD source, respectively.

$$D = \frac{k\lambda}{\beta \cos \theta} \tag{1}$$

Photocatalytic Evaluation

The photocatalytic activity of the prepared BST was evaluated through MB photodegradation. First, 1 gram of MB powder was dissolved in 1000 ml of distilled water, producing 10 ppm of MB solution. The MB solution was then measured at a wavelength range of 350 – 800 nm to determine the initial absorbance of the solution. After that, 0.5 grams of the prepared BST were dissolved in 10 mL of the MB solution. Before irradiation, the MB-photocatalyst solutions were stirred in the dark for 30 min to reach adsorption-desorption equilibrium. The solutions were then exposed under UV light for 5 hours. To investigate the effects of irradiation times

on the photodegradation, the MB solution with $Ba_{0.5}Sr_{0.5}TiO_3$ was irradiated for 3, 5, and 6 hours. All exposed solutions were examined with a UV-Vis Spectrophotometer to measure the absorbance. The percentages of dye degradation by the BST photocatalysts with different Sr contents were then estimated using Equation $2^{[2]}$. In which DP, A_o , and A_t are the dye degradation percentage, the initial absorbance, and the absorbance after time t, respectively.

$$DP = \frac{Ao - At}{Ao} \times 100\% \tag{2}$$

RESULTS AND DISCUSSION

Figure 1a shows the diffraction patterns of prepared samples with distinct Sr contents. The patterns were matched with the International Center for Diffraction Data (ICDD) database PDF #792263, confirming the crystal structure of BST. The diffraction peaks appeared to correspond to the crystal planes of (100), (110), (111), (200), (211), (220), and (310), validating the cubic structure of BST with the *Pm3m* space group. The figure shows a right shift with increased Sr contents at the highest peaks (110) (Figure 1b). Besides, the absence of the splitting peaks between planes (200) and (022) at 2θ about 45° (Figure 1c) denotes the formation of cubic BST. Similar to (110), the planes (200) also demonstrate the right shifts with the higher Sr concentration. The shift indicates that Sr has replaced Ba sites, leading to lattice alteration. However, the peaks marked (*) were detected as impurities that matched the ICDD PDF database #190125. They were identified as BaC₂O₄, which resulted from the reaction between Ba(OH)₂ and CO₂ in the air during the mixing process.

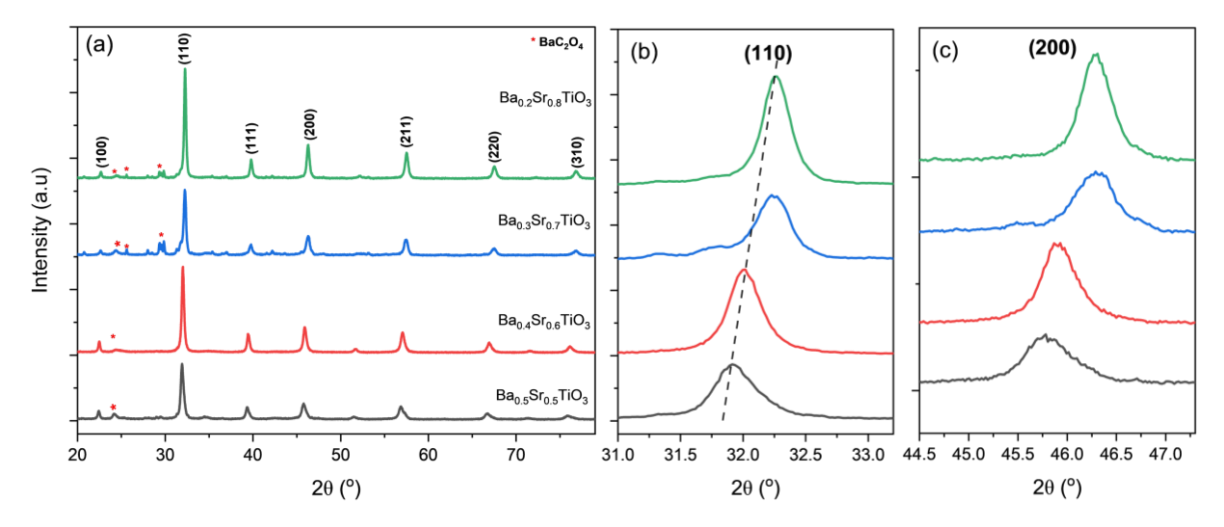


Figure 1. Diffraction patterns of the prepared BST samples with distinct Ba/Sr ratios and the right shift of (110) peaks due to higher Sr content

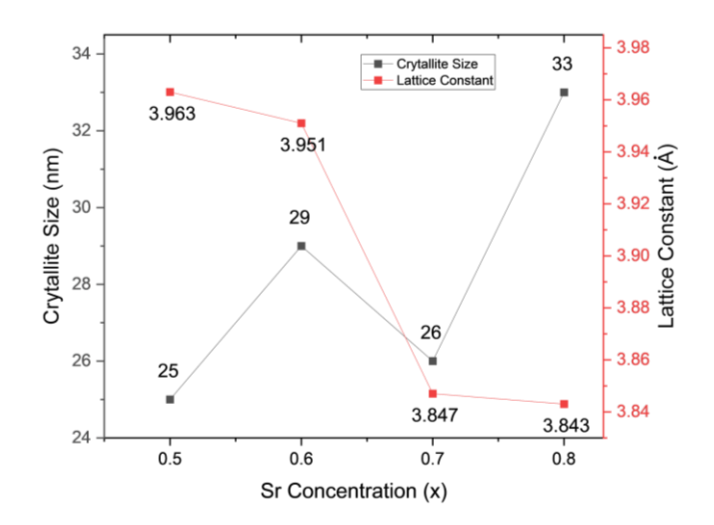


Figure 2. Lattice constants and crystallite sizes of the prepared BST

According to Figure 2, the lattice constants of BST decreased with increasing Sr concentration. This decrease may be due to the replacement of Ba^{2+} with Sr^{2+} ions, possessing a different ionic radius (Sr =1.16 Å < Ba=1.36 Å) [18]. In addition, the crystallite size of BST tends to enlarge with increasing Sr concentration, except at x=0.7. The smallest crystallite size at x = 0.7 is considered due to maximum lattice distortion inhibiting crystal growth. At this composition, increased internal strain promotes nucleation but suppresses crystal enlargement, as reported by Rashad et al^[28]. In contrast, at x = 0.5 - 0.6, the structure remains relatively stable, while it tends toward a more symmetric phase at x = 0.8, allowing larger crystals to form^[29, 30].

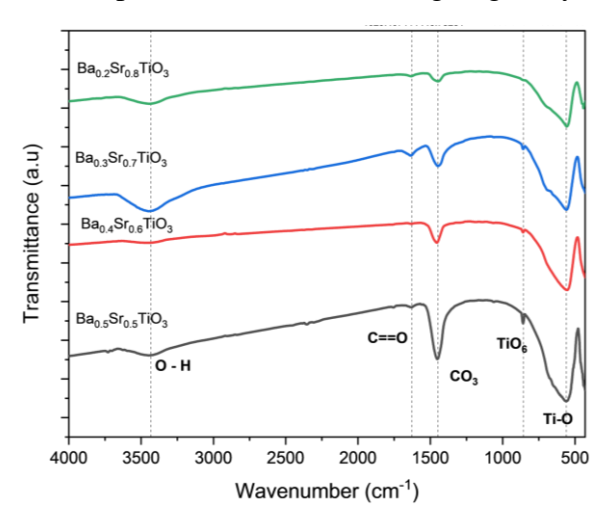


Figure 3. FTIR spectra of the prepared BST

Figure 3 depicts the FTIR spectra of the prepared BST samples. The prominent peaks detected at about 555 – 558 cm⁻¹ wavenumbers were attributed to the stretching vibration of the BO₆ octahedron. B in BO₆ denotes the B site in the ABO₃ perovskite structure, referring to the Ti atom in TiO₆. Hence, these peaks can be ascribed to the vibration of Ti–O octahedra in titanate compounds ^[18, 31]. The peaks at about 858 – 859 cm⁻¹ were related to the vibration of the metal-oxygen bond ^[32]. This peak usually describes the vibrational modes of the TiO₆ bond. In the context of BST, it is also typical of the perovskite structure of BaTiO₃ and its strontium-substituted variations. Besides, metal-oxygen absorption bands observed in FTIR spectra confirm the existence of the perovskite structure ^[18]. The vibrational peaks at around 1448 – 1455 cm⁻¹ were associated with the anti-symmetric stretching and bending vibrations of

carbonate groups (CO₃). These peaks are caused by impurities formed during the synthesis process due to the reactions between raw materials under room conditions $^{[3,27,32]}$. The peaks at about 1633 cm⁻¹ denote the carbonyl groups in the samples $^{[31-33]}$. Meanwhile, the vibrational peaks at about 3442 - 3446 cm⁻¹ were related to O-H groups originating from the water absorption on the sample's surface $^{[31,33]}$.

The photocatalytic activities of the prepared BST samples were assessed through MB degradation under UV light (Figure 4a). It demonstrated that the absorbances of the BST samples with distinct Sr ratios were much lower than that of the sole MB after 5 hours of irradiation. The reduced absorbances indicate higher degradation efficiency and better photocatalytic performance^[2]. Figure 4b displays the degradation percentages for MB by the BST photocatalysts. After 5 hours of irradiation, the degradation percentages of MB by Ba_{0.5}Sr_{0.5}TiO₃, Ba_{0.4}Sr_{0.6}TiO₃, Ba_{0.3}Sr_{0.7}TiO₃, and Ba_{0.2}Sr_{0.8}TiO₃ were 7, 27, 41, and 25 %, respectively (Figure 4b). The photocatalytic performances of Ba_{0.5}Sr_{0.5}TiO₃, Ba_{0.4}Sr_{0.6}TiO₃, and Ba_{0.2}Sr_{0.8}TiO₃ were relatively low. In general, the photocatalytic activity of the BST improved with the increase in Sr content to Ba_{0.3}Sr_{0.7}TiO₃, after which the activity decreased.

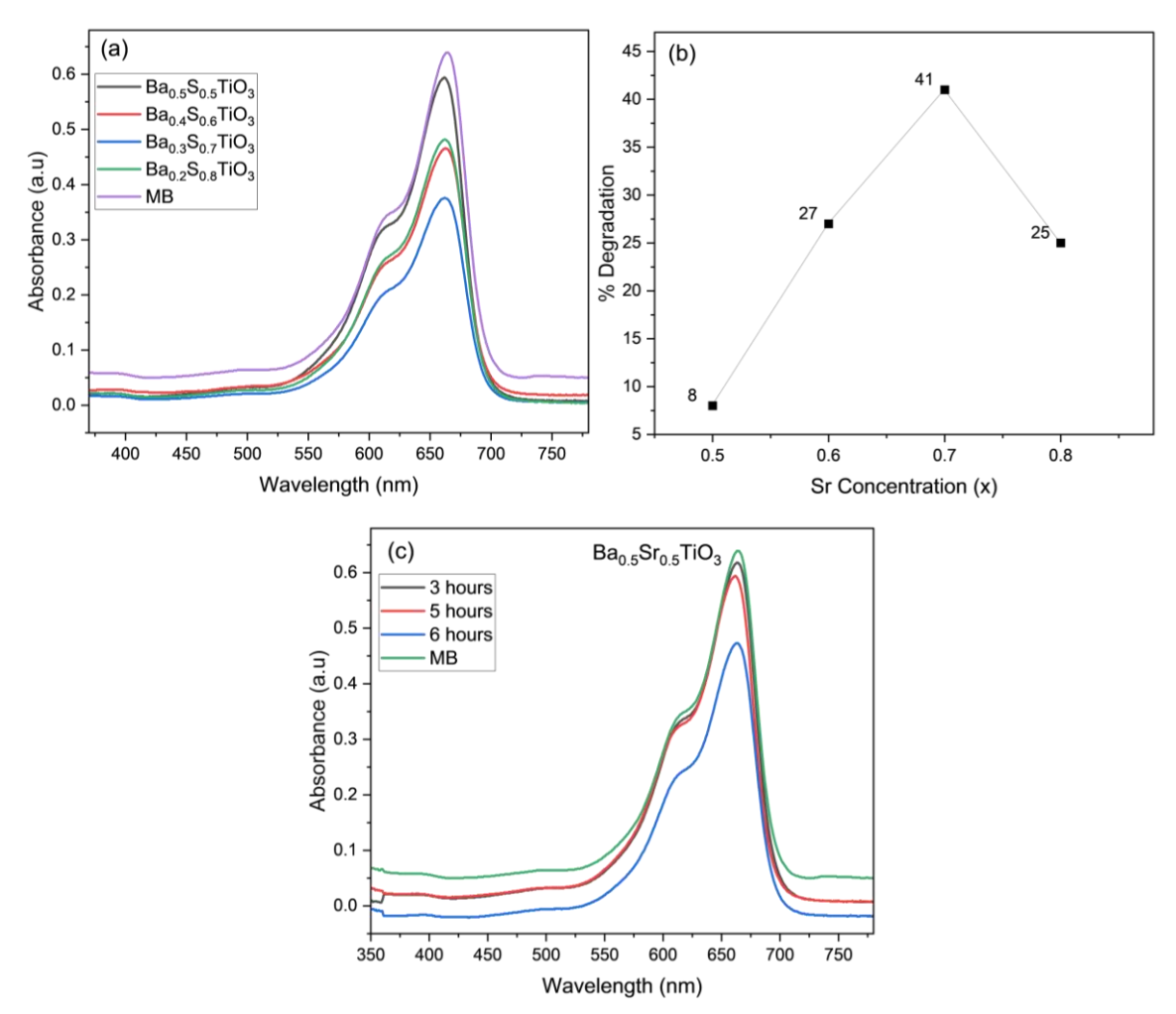


Figure 4. (a) Absorbance of degraded MB by the prepared BST after 5 hours of UV irradiation, (b) MB degradation percentages as a function of Sr contents, and (c) the effect of UV irradiation times on MB degradation

Bhat et al. ^[16] also reported a similar trend through a Density Functional Theory (DFT) study and in the cases of Rh-doped BTO. This phenomenon can be related to different Ba/Sr ratios in the BST structure. The crystal structure of BST materials will experience lattice change and

distortion due to the various amounts of $Sr^{[15,\,31]}$. Because Sr^{2+} has a smaller ionic radius than Ba^{2+} , more Sr induces a smaller lattice size (Figure 2). This can cause strain in the lattice and affect the geometry of the TiO_6 octahedron (the main structure contributing to photocatalytic activity) $^{[34,\,35]}$. The distortion in the TiO_6 octahedron in the BST structure can also create an internal field that helps charge separation $^{[34,\,36]}$. Hence, at $Ba_{0.5}Sr_{0.5}TiO_3$, $Ba_{0.4}Sr_{0.6}TiO_3$, and $Ba_{0.3}Sr_{0.7}TiO_3$ (x=0.5-0.7), the structure is more distorted $^{[15,\,27]}$, which can help electron-hole separation so that the photodegradation efficiency is enhanced. However, at $Ba_{0.2}Sr_{0.8}TiO_3$ (x=0.8), the structure can be said to be almost symmetrical (towards perfect cubic) $^{[15,\,37]}$ with minimal distortion, so that the charge separation becomes inefficient $^{[38]}$. This causes the electron-hole recombination centers to increase, so the photodegradation efficiency is reduced.

Furthermore, the study of Han et al., concerning the impact of Sr content (x = 0.1 - 0.5) on photocatalytic activity of $Ba_{1-x}Sr_xTiO_3$ under visible light, also supports that crystal phase and energy band are key in influencing and optimizing the photocatalysts ^[15]. The phase was reported to change from tetragonal to cubic, and the band gap improved with increasing Sr. Further, the photocatalytic activity (tetracycline HCl degradation) was enhanced with increasing Sr due to microstructural and phase changes. Hence, this study and Han et al.'s research showed that the concentration of Sr^{2+} affected the crystal structure and photocatalytic activity.

Additionally, Liu et al. ^[26] reported the synthesis of $Ba_{1-x}Sr_xTiO_3$ (x=0 - 0.3) nanopowders and the impact of Sr doping on their tribocatalytic performance in degrading RhB pollutants. Although their primary focus was tribocatalysis (catalytic activity due to friction), the study demonstrated a similar trend. The yields revealed that photocatalytic performance was enhanced to an optimum at x=0.2 and then declined with increasing doping. This indicates that optimum photocatalytic activity can be achieved at a certain doping level, and may decrease if the structure becomes too symmetric or the lattice distortion is reduced at excessive doping.

Thus, the results of this study, exhibiting an increase in photocatalytic activity at x = 0.5 to 0.7, followed by a decrease at x = 0.8, are consistent with previous literature. The decline in activity at x = 0.8 can be explained by the reduction in lattice distortion due to a more symmetrical structure, as reported in similar studies^[16, 39]. Thus, these findings reinforce the understanding that there is an optimal limit in Sr^{2+} doping of BST to achieve maximum photocatalytic performance. Moreover, these results also fill the gaps in previous research, which mainly focused on low Sr concentrations, by exploring the effects of higher Sr levels.

Figure 4c shows that the absorbances in Ba_{0.5}Sr_{0.5}TiO₃ declined with the longer irradiation times, denoting the improved photocatalytic activity of the BST photocatalysts. The longer irradiation provides more opportunities for the photocatalysts to absorb more energy from light. This will facilitate more redox reactions during the photocatalysis process, causing more hydroxyl radicals to be released and further improving the degradation efficiency.

Overall, the photocatalytic process by photocatalysts to degrade organic pollutants can be explained as follows^[4, 8, 16]. When the photocatalysts are exposed to light energy (hv), pairs of electrons (in the conduction band) and holes (in the valence band) will be produced on the surface of the material. Then, the electron and hole pairs will react with other molecules in the solutions to produce radical compounds (redox reactions). Electrons react with O_2 to produce superoxide radicals (O_2). Meanwhile, holes interact with O_2 to generate hydroxyl radicals (O_2). The hydroxyl radicals can directly oxidize dye molecules. Meanwhile, O_2 will react with water and hydrogen peroxide (O_2), which decay into O_2 in the presence of light. The

active species formed, such as •OH (most dominant) and \bullet O₂⁻, respond with dye and decay to CO₂ and water, leaving harmless products.

Ultimately, this research provides new insights into the optimal Sr^{2+} doping range (x=0.7) for enhancing photocatalytic activity. This is significant because many previous studies focused only up to x=0.5. These findings fill a gap in the literature and demonstrate that excessive doping (x>0.7) degrades performance due to decreased lattice distortion. However, future research should include a detailed analysis of the lattice distortion and bandgap energy using appropriate techniques to reinforce the justification of the relationship between doping, structural changes, and photocatalytic activity.

CONCLUSION

 $Ba_{1-x}Sr_xTiO_3$ photocatalysts with varying Sr^{2+} concentrations were synthesized via coprecipitation. Increasing Sr content reduced lattice constants and increased crystallite size. Photocatalytic activity improved at x=0.5–0.7, attributed to enhanced lattice distortion, but declined at x=0.8 due to increased symmetrical structure. $Ba_{0.3}Sr_{0.7}TiO_3$ showed the highest MB degradation, indicating the optimal composition and a new finding in this research. These results highlight the significant influence of Sr doping on structural and photocatalytic properties. Future work should analyze lattice distortion and bandgap characteristics using appropriate techniques to clarify the relationship between doping, structure, and performance in BST-based photocatalysts.

ACKNOWLEDGMENTS

The authors thank the 2024 Research Group Grant by Universitas Sebelas Maret, with contract no 194.2/UN27.22/PT.01.03/2024, for funding this research.

REFERENCES

- Liu S., Qiu H., Yamamoto A., Yoshida H. 2024. Barium titanate photocatalysts with silver-manganese dual cocatalyst for carbon dioxide reduction with water. *Dalton Trans.* 53(25), 10712-9. Epub 2024/06/13. doi: 10.1039/d4dt01147c. PubMed PMID: 38869439.
- 2 Robles-Cortes A. I., Flores-Ramírez D., Armienta-Millán C., Romero-Ibarra I. C., Ortiz-Landeros J. 2023. A facile synthesis of bismuth-modified barium titanate as photocatalyst for degradation of rhodamine B. *MRS Advances*. 8(23), 1330-5. doi: 10.1557/s43580-023-00685-0.
- Ata S., Shaheen I., Aslam H., Mohsin I. U., Alwadai N., Huwayz M. A., et al. 2023. Barium and strontium doped La-based perovskite synthesis via sol-gel route and photocatalytic activity evaluation for methylene blue. *Results in Physics*. 45106235. doi: 10.1016/j.rinp.2023.106235.
- 4 Iriani Y., Puspita N. F. S., Sandi D. K., Nurosyid F., Suryana R., Fasquelle D. 2024. The Improved Photocatalytic Performance of Strontium Titanate (STO) Powder Induced by Lanthanum Dopants. *Iranian Journal of Materials Science and Engineering*. 21(4), 1-10. doi: 10.22068/ijmse.3645.
- 5 Shu-Xiang G. U. I., Xian-Lin D., Chao-Liang M. A. O., Hao L. I., Yang B. A. I., Tao Z. 2015. Fabrication of Barium Strontium Titanate Nanophotocatalysts with Gridding Structures and Their Photocatalytic Activities. *Journal of Inorganic Materials*. *30*(12). doi: 10.15541/jim20150245.
- Danish M. S. S., Estrella L. L., Alemaida I. M. A., Lisin A., Moiseev N., Ahmadi M., et al. 2021. Photocatalytic Applications of Metal Oxides for Sustainable Environmental Remediation. *Metals*. 11(1). doi: 10.3390/met11010080.
- Kumari H., Sonia, Suman, Ranga R., Chahal S., Devi S., et al. 2023. A Review on Photocatalysis Used For Wastewater Treatment: Dye Degradation. *Water Air Soil Pollut.* 234(6), 349. Epub 2023/06/05. doi: 10.1007/s11270-023-06359-9. PubMed PMID: 37275322; PubMed Central PMCID: PMCPMC10212744.

- 8 Vaz T., More A. S., Fernandes J., Gurav S. M. 2021. Influence of Ba Substitution in SrTiO₃ Perovskite Studies of Photocatalysis and Catalytic Biginelli Reaction. *Journal of Advanced Scientific Research*. 12(2), 178 84.
- 9 Lariski F. M., Zangina T., Ndikilar C. E., Mohammed J. 2023. Advances in the synthesis, characterizations and applications of barium titanate. A review. *Dutse Journal of Pure and Applied Sciences*. *9*(3a), 117-36. doi: 10.4314/dujopas.v9i3a.13.
- 10 Iriani Y., Suherman B., Dianisa Khoirum S., Nurosyid F., Handoko E. 2024. Microstructure, Atomic Bonds, and Dielectric Characteristics of Neodymium (Nd)-doped Barium Titanate. *Evergreen.* 11(3), 2063-70. doi: 10.5109/7236851.
- Iriani Y., Suherman B., Sandi D. K., Nurosyid F., Khairuddin, Handoko E., et al. 2024. Structural Modification and Dielectric Property of Bi-Doped BaTiO₃ (Ba_{1-x}Bi_xTiO₃) Ceramics with co-Precipitation Technique. *Integrated Ferroelectrics*. 240(1), 140-8. doi: 10.1080/10584587.2023.2296318.
- Abedi M., Basheer H. S., Lakatos L., Kukovecz A., Konya Z., Gyulavari T., et al. 2024. Influence of Rapid Heat Treatment on the Photocatalytic Activity and Stability of Barium Titanates Against a Broad Range of Pollutants. *Molecules*. 29(22), 5350. Epub 2024/11/27. doi: 10.3390/molecules29225350. PubMed PMID: 39598741; PubMed Central PMCID: PMCPMC11596716.
- Jebali S., Meftah M., Mejri C., Ben Haj Amara A., Oueslati W. 2023. Enhancement of Photocatalytic Activity and Microstructural Growth of Cobalt-Substituted Ba_{1-x}Co_xTiO₃ Heterostructure. *ChemEngineering*. 7(3), 43. doi: 10.3390/chemengineering7030043.
- Al-Wasidi A. S., Abdelrahman E. A. 2023. Significant photocatalytic decomposition of malachite green dye in aqueous solutions utilizing facilely synthesized barium titanate nanoparticles. *Discov Nano.* 18(1), 97. Epub 2023/07/29. doi: 10.1186/s11671-023-03873-x. PubMed PMID: 37507521; PubMed Central PMCID: PMCPMC10382382.
- Han Y., Wang S., Li M., Gao H., Han M., Yang H., et al. 2023. Strontium-induced phase, energy band and microstructure regulation in Ba_{1-x}Sr_xTiO₃ photocatalysts for boosting visible-light photocatalytic activity. *Catalysis Science & Technology*. *13*(9), 2841-54. doi: 10.1039/d3cy00278k.
- Bhat D. K., Bantawal H., Shenoy U. S. 2020. Rhodium doping augments photocatalytic activity of barium titanate: effect of electronic structure engineering. *Nanoscale Advances*. 2(12), 5688-98. Epub 2020/11/05. doi: 10.1039/d0na00702a. PubMed PMID: 36133860; PubMed Central PMCID: PMCPMC9418416.
- Mohan H., Vadivel S., Shin T. 2023. Sonophotocatalytic water splitting by BaTiO₃@SrTiO₃ core shell nanowires. *Ultrason Sonochem.* 101106650. Epub 2023/10/23. doi: 10.1016/j.ultsonch.2023.106650. PubMed PMID: 37866137; PubMed Central PMCID: PMCPMC10623364.
- Moussi R., Bougoffa A., Trabelsi A., Dhahri E., M.P.F.Graça, Valente M. A., et al. 2021. Effect of Sr-substitution on structure, dielectric relaxation and conduction phenomenon of BaTiO₃ perovskite material. *Journal of Materials Science: Materials in Electronics*. 32(9), 11453-66. doi: 10.1007/s10854-021-05604-3.
- Elmahgary M. G., Mahran A. M., Ganoub M., Abdellatif S. O. 2023. Optical investigation and computational modelling of BaTiO₃ for optoelectronic devices applications. *Sci Rep. 13*(1), 4761. Epub 2023/03/25. doi: 10.1038/s41598-023-31652-2. PubMed PMID: 36959231; PubMed Central PMCID: PMCPMC10036486.
- 20 Rohj R. K., Hossain A., Mahadevan P., Sarma D. D. 2021. Band Gap Reduction in Ferroelectric BaTiO₃ Through Heterovalent Cu-Te Co-Doping for Visible-Light Photocatalysis. *Front Chem.* 9682979. Epub 2021/06/11. doi: 10.3389/fchem.2021.682979. PubMed PMID: 34109158; PubMed Central PMCID: PMCPMC8181162.
- Ramakanth S., James Raju K. C. 2014. Band gap narrowing in BaTiO₃ nanoparticles facilitated by multiple mechanisms. *Journal of Applied Physics*. 115(17), 173507. doi: 10.1063/1.4871776.
- Zidi Y., Khaldi O., Patru R. E., Leonat L. N., Enculescu M., Toma V., et al. 2025. Experimental and theoretical perspective on band gap modulation in Sr²⁺ modified BaTiO₃ capacitors. *Ceramics International*. *51*(13), 18166-77. doi: 10.1016/j.ceramint.2025.01.591.

- Nassereddine Y., Benyoussef M., Asbani B., El Marssi M., Jouiad M. 2023. Recent Advances toward Enhanced Photocatalytic Proprieties of BiFeO₃-Based Materials. *Nanomaterials (Basel)*. *14*(1), 51. Epub 2024/01/11. doi: 10.3390/nano14010051. PubMed PMID: 38202506; PubMed Central PMCID: PMCPMC10780865.
- Alomair N. A., Al-Aqeel N. S., Alabbad S. S., Kochkar H., Berhault G., Younas M., et al. 2023. The Role of the Ferroelectric Polarization in the Enhancement of the Photocatalytic Response of Copper-Doped Graphene Oxide-TiO₂ Nanotubes through the Addition of Strontium. *ACS Omega*. 8(9), 8303-19. Epub 2023/03/14. doi: 10.1021/acsomega.2c06717. PubMed PMID: 36910964; PubMed Central PMCID: PMCPMC9996589.
- RaeisianAsl M., Jouybar S., Sarabadani Tafreshi S., Naji L. 2025. Exploring the key features for enhanced SrTiO₃ functionality: A comprehensive overview. *Materials Today Sustainability*. 29(2025), 101072. doi: 10.1016/j.mtsust.2025.101072.
- 26 Liu S., Yang Y., Hu Y., Rao W. F. 2023. Effect of Strontium Substitution on the Tribocatalytic Performance of Barium Titanate. *Materials (Basel)*. 16(8), 3160. Epub 2023/04/28. doi: 10.3390/ma16083160. PubMed PMID: 37109994; PubMed Central PMCID: PMCPMC10143700.
- 27 Liu K., Mi L., Wang H., Xiong X., Zhang K., Wang B. 2021. Preparation of Ba_{1-x}Sr_xTiO₃ by the sol-gel assisted solid phase method: Study on its formation mechanism and photocatalytic hydrogen production performance. *Ceramics International*. 47(15), 22055-64. doi: 10.1016/j.ceramint.2021.04.226.
- Rashad M. M., Turky A. O., Kandil A. T. 2013. Optical and electrical properties of $Ba_{1-x}Sr_xTiO_3$ nanopowders at different Sr^{2+} ion content. *Journal of Materials Science: Materials in Electronics*. 24(9), 3284-91. doi: 10.1007/s10854-013-1244-9.
- Ahn H., Lee E., Cho Y., Bae D., Park H., Yang J., et al. 2021. Ferroelectric Transition in Sr- and W-Doped BaTiO₃ Solid Solutions. *Applied Sciences*. 11(15), 6760. doi: 10.3390/app11156760.
- 30 Kacimi-Naciri H., Rguiti M., Mabrouk A., Courtois C., Ben Achour M. A., Lorgouilloux Y., et al. 2025. DFT-based and experimental study on Sr-doped BaTiO₃: Impacts on piezoelectric and ferroelectric performance. *Ceramics International*. *51*(17), 23801-13. doi: 10.1016/j.ceramint.2025.03.069.
- Devi L. R., Naorem B., Choudhary A., Sharma H. B. 2024. Influence of Sr²⁺ ion content on the structural and electrical properties of Ba_{1-x}Sr_xTiO₃ nanopowders. *Journal of Materials Science: Materials in Electronics*. *35*(32). doi: 10.1007/s10854-024-13841-5.
- Hussein M. M., Saafan S. A., Abosheiasha H. F., Kamal A. A., Mahmoud A. E.-r., Zhou D., et al. 2023. Structural and dielectric characterization of synthesized nano-BSTO/PVDF composites for smart sensor applications. *Materials Advances*. 4(22), 5605-17. doi: 10.1039/d3ma00437f.
- Zheng Y., Feng G., Chen C., Jiang F., Zhao C., Yuan Q., et al. 2025. Improved piezo-photocatalysis performance of Ba_{1-x}Sr_xTiO₃ nanopowders via synergistically optimizing phase ratio, defects and polarization. *Journal of Alloys and Compounds*. 1011(2025), 178348. doi: 10.1016/j.jallcom.2024.178348.
- Malik J., Kumar S., Srivastava P., Bag M., Mandal T. K. 2021. Cation disorder and octahedral distortion control of internal electric field, band bending and carrier lifetime in Aurivillius perovskite solid solutions for enhanced photocatalytic activity. *Materials Advances*. 2(14), 4832-42. doi: 10.1039/d1ma00304f.
- Dhole S., Chen A., Nie W., Park B., Jia Q. 2022. Strain Engineering: A Pathway for Tunable Functionalities of Perovskite Metal Oxide Films. *Nanomaterials (Basel)*. *12*(5). Epub 2022/03/11. doi: 10.3390/nano12050835. PubMed PMID: 35269323; PubMed Central PMCID: PMCPMC8912649.
- Hu Y., Pan Y., Wang Z., Lin T., Gao Y., Luo B., et al. 2020. Lattice distortion induced internal electric field in TiO₂ photoelectrode for efficient charge separation and transfer. *Nature Communications*. *11*(1), 2129. Epub 2020/05/03. doi: 10.1038/s41467-020-15993-4. PubMed PMID: 32358565; PubMed Central PMCID: PMCPMC7195485.
- Bantawal H., Shenoy U. S., Bhat D. K. 2018. Tuning the Photocatalytic Activity of SrTiO₃ by Varying the Sr/Ti Ratio: Unusual Effect of Viscosity of the Synthesis Medium. *The Journal of Physical Chemistry C.* 122(34), 20027-33. doi: 10.1021/acs.jpcc.8b06514.

- Wang Y. Effect of Polar Structure on Photocatalytic Properties of Oxide Powders and Films. London: Queen Mary, University of London; 2018.
- 39 Saravanan R., Mangaiyarkkarasi J. 2015. Synthesis and analysis of electron density distribution in Ba_{1-x}Sr_xTiO₃ ceramics. *Journal of Materials Science: Materials in Electronics.* 27(3), 2523-33. doi: 10.1007/s10854-015-4053-5.